JOURNAL OF SPACECRAFT AND ROCKETS
Vol. 32, No. 6, November–December 1995

Clementine Attitude Determination and Control System

Paul DeLaHunt,* Steve Gates,† and Marv Levenson‡
U.S. Naval Research Laboratory, Washington, D.C. 20375
and
Glenn Creamer§
Swales and Associates Inc., Beltsville, Maryland 20705

The Clementine spacecraft, launched in January 1994, completed a two-month lunar mapping mission, recording high-resolution multispectral images of the lunar surface in unprecedented detail. Mission requirements on the attitude determination and control system included knowledge to within 0.03 deg and control to within 0.05 deg. The typical spacecraft attitude determination system, employing expensive narrow-field-of-view star cameras, highly accurate inertial measurement units, and assorted coarse attitude acquisition sensors, was replaced by an all-new lightweight state-of-the-art sensor suite to meet low-cost, low-weight, and compressed schedule objectives. The sensor suite, which consisted of two wide-field-of-view star cameras and two inertial measurement units incorporating fiber-optic and ring-laser gyroscopes, was delivered in nine months and provided a weight saving of 90% and a cost saving of 75% in comparison with similar systems. A newly developed lightweight reaction wheel, with a weight saving of 50% in comparison with wheels of similar momentum storage capability, was used for fine attitude control. The Clementine mission provided the first space flight for each of these components. Only two anomalies were experienced: a large drift in gyroscope bias along one axis, and a nondestructive single-event latchup in one inertial measurement unit.

I. Introduction and Mission Overview

CLEMENTINE, the Deep Space Program Science Experiment spacecraft, was launched on Jan. 25, 1994. Clementine's primary objective was to demonstrate in space the most advanced lightweight imaging sensors and component technologies for the next generation of lightweight Department of Defense spacecraft. As a secondary objective, Clementine was to be the first U.S. spacecraft to return to the moon in 22 years and was tasked to obtain the first complete high-resolution mapping of the lunar surface. After completing this two-month assignment, the spacecraft was to alter course for a close fly-by and observation of the near-Earth asteroid 1620 Geographos. The spacecraft carried a suite of high-resolution imaging cameras operating in the ultraviolet, visible, and infrared spectral regions, as well as two star cameras for imaging and attitude determination. Specific characteristics of the sensor payload as well as general descriptions and objectives of the Clementine mission are provided in Refs. 1 and 2.

Clementine achieved lunar orbit on Feb. 21, 1994, through a series of multiple phasing loops and spent approximately two months in two separate lunar orbits, during which time it successfully mapped the entire surface of the moon in ultraviolet, visible, and near-infrared spectra. Clementine was then scheduled to travel towards Geographos after entering a highly elliptical orbit about the earth with a lunar gravity assist. However, on May 7, 1994, an onboard computer malfunction activated several thrusters, expelling the remaining attitude control fuel. As a result, the asteroid fly-by phase of the mission could not be achieved. A complete description of the nominal Clementine mission astrodynamics is provided in Ref. 3.

In this paper we describe the design and on-orbit performance of an all-new attitude determination and control system (ADCS) architecture using lightweight state-of-the-art wide-field-of-view star cameras and lightweight inertial measurement units incorporating fiber-optic and ring-laser gyroscope technology for the first time on a spacecraft. The Clementine spacecraft went from concept to launch in a 22-month development cycle, far shorter than is typical for this challenging a mission. Compressing the development cycle was the primary factor in meeting cost containment goals set by the sponsor.

Descriptions of the vehicle configurations, sensor payload, and spacecraft characteristics are provided in Sec. II. Section III describes the attitude determination and control system components. The attitude determination, three-axis control, and spin stabilization control systems are described in Sec. IV. Section V discusses on-orbit performance and hardware anomalies. Finally, some concluding remarks are given in Sec. VI.

II. Spacecraft Configuration and Characteristics

Clementine had two primary configurations during its mission. It was configured as shown in Fig. 1 until the solid-rocket-motor burn for low-Earth-orbit (LEO) departure. In this configuration the two solar array panels were in their stowed positions and the solid rocket motor was attached and fully loaded. The spacecraft was three-axis-stabilized for a one-week checkout period prior to being spin-stabilized for 4 h, leading up to a 63-s burn of the solid rocket motor. After completion of the burn the spacecraft was reconfigured as shown in Fig. 2. In this configuration Clementine was three-axis-stabilized with the two solar array panels deployed and the

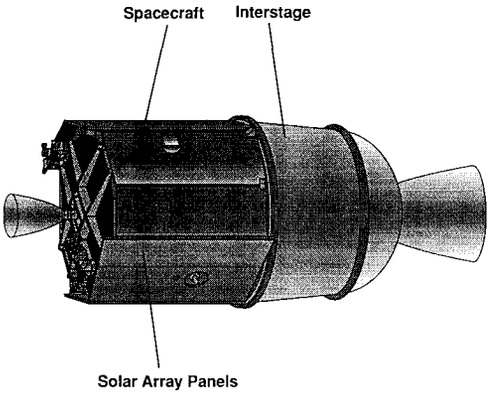

Fig. 1 Spacecraft configuration in LEO.

Received Sept. 2, 1994; revision received Jan. 9, 1995; accepted for publication Jan. 23, 1995. This paper is declared a work of the U.S. Government and is not subject to copyright protection in the United States.

*Subsystem Lead Engineer, Spacecraft Attitude Control Section. Member AIAA.

†Aerospace Engineer, Spacecraft Attitude Control Section. Member AIAA.

‡Section Head, Spacecraft Attitude Control Section. Member AIAA.

§Senior Control System Engineer. Member AIAA.

Table 1 Masses and moments of inertia

Characteristic	Configuration		
	LEO	Deployed	
	(Wet)	(Wet)	(Dry)
Mass, kg	1647	456	233
Inertia, kg · m^2			
I_{xx}	199	93	66
I_{yy}	733	80	56
I_{zz}	736	107	77

Table 2 Science payload masses

Component	Mass, kg
Star tracker cameras (2)	0.3
UV–visible camera	0.5
Near-IR camera	1.9
Long wave IR camera	1.8
High resolution camera	1.3
Laser transmitter	0.6
Charged particle telescope	0.2
Dosimeters (4)	0.1
Radiation experiment	0.7
Orbital meteoroid and debris counting experiment	0.6
Total	8.0

Table 3 Spacecraft characteristics

Characteristic	Data
Mass	456 kg (wet)
Power	360 W at 1 AU
Size	1.14-m diam ×1.88-m length
Miscellaneous	Three-axis stabilized
	Single-axis gimbaled GaAs solar arrays
	Fixed 1.1-m high-gain antenna
	Fixed payload sensors
	Combined active and passive thermal design
Telemetry	S-Band rf link to NASA DSN and DoD tracking stations
Data rate	Downlink selectable between 0.125 and 128 kb/s
Onboard storage	1.9-Gbit solid-state recorder
Propulsion	4865-m/s ΔV
	Bipropellant (MMH and N_2O_4) 489-N ΔV motor
	Monopropellant (hydrazine) with ten 5.3-N and two 22.7-N ACS thrusters
	STAR 37FM kick motor

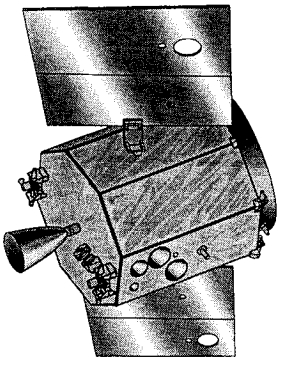

Fig. 2 Spacecraft configuration during lunar mapping.

motor case separated. It maintained this configuration throughout the remainder of the mission. Spacecraft mass and inertias for each configuration are provided in Table 1. The science payload mass properties are provided in Table 2, and some additional spacecraft characteristics are given in Table 3.

With the exception of the solid-rocket-motor burn, all orbit changes were achieved with a bipropellant reaction control system using monomethyl hydrazine and nitrogen tetroxide with 134,000 lbf · s of total impulse, and a 110-lbf ΔV motor. This motor, along with the layout of the attitude control thrusters, is shown in Fig. 3.

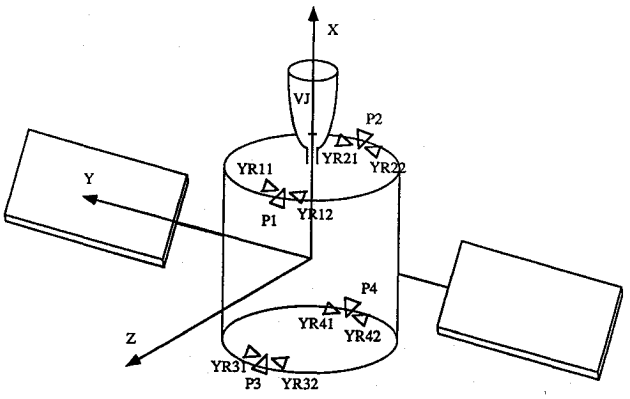

Fig. 3 Thruster configuration of attitude control system.

The 110-lbf ΔV thruster is denoted by VJ, the two 5-lbf thrusters are denoted by P1 and P2, and the other ten are 1-lbf thrusters. The attitude control thrusters were run off a separate blowdown hydrazine tank, which resulted in the force of the 5-lbf thrusters decreasing to 2.1 lbf, and the force of the 1-lbf thrusters decreasing to 0.4 lbf, as the hydrazine was consumed. The thrusters were used for attitude control during ΔV burns, momentum management burns, asteroid fly-by slews, spin rate changes, spin axis precession, and active nutation control. In the LEO configuration, the solid rocket motor covered the six $-X$ thrusters.

III. Component Selection and Hardware Description

Component selection for space missions is typically based on performance, space qualification status, flight experience, size, weight, and cost. Each of these factors may be weighted differently according to the type of program or sponsor. For most spacecraft, space qualification status and flight experience are usually the greatest concern, so much so that new lightweight state-of-the-art systems are often not considered. However, for Clementine, light weight and compact size were the most significant factors. With this selection a higher level of risk was accepted. The level of risk was then minimized through selected redundancy.

The attitude knowledge requirement was 3 deg in LEO, based on pointing requirements of the solid-rocket-motor burn; 0.25 deg for other ΔV maneuvers; and 0.03 deg for image data collection. To meet the tight requirement of image data collection during the cruise to the moon, lunar mapping, and cruise to and fly-by of the asteroid, it was necessary to use a combination of star cameras and gyroscopes. This configuration of sensors is typically made up of expensive, highly accurate, narrow-field-of-view star cameras and low-drift-rate gyroscopes, and assorted coarse attitude sensors for initial acquisition and transition to the fine pointing system. For this mission, with its weight, schedule, and cost limitations, a new state-of-the-art configuration of star cameras and gyroscopes was implemented.

The attitude determination system was based on a wide-field-of-view, lightweight star camera capable of providing three-axis attitude determination with a single image. An inertial measurement unit with low-performance gyroscopes for attitude propagation between star-camera updates was selected. The capability of the star camera to provide three-axis attitude determination without a priori knowledge of vehicle attitude avoided the need for coarse attitude acquisition sensors. Acquisition of attitude was performed simply by taking a star-camera image from any attitude. If body rates exceeded 0.25 deg/s, the maximum rate allowed for proper star-camera operation, then the inertial measurement units and control actuators were used to reduce body rates to within the star-camera rate capability.

Clementine's attitude was updated by the star camera, nominally every 10 s, through the following process. A snapshot was taken by a star camera, which was passed to the spacecraft controller in the form of a digital image. The spacecraft controller processed the digital image and identified the brightest objects. Triangles were created from those objects, and matched to an onboard star catalog, to generate a measured attitude quaternion and quality factor. Finally, the measured attitude quaternion was passed through a Kalman filter

Table 4 LLNL ST camera specification

Characteristic	Value
Mass	364 g
Size	4.6 × 4.6 × 5.2 in.
Power dissipation	4.5 W
Spectral range	0.4–1.1 μm
Field of view	43.2 × 28.4 deg
IFOV	1.28 mrad (0.073 deg)
Accuracy	150 × 150 × 450 μrad
Number of pixels	576 × 384
Integration time	200 ms
Sensitivity	SNR = 20 at $M_v = 4.5$

to estimate the vehicle attitude. The star camera included the sensor head and separate image-processing software loaded in the spacecraft controller.

Two star cameras with no overlapping coverage were used to ensure attitude updates throughout the mission. Because of sun interference, only one star camera could be used at a time during lunar mapping. In spite of this, there was still an extremely high percentage of successful quaternion matches. During LEO operations, the attitude was updated with alternating star cameras. This mode of operation gave approximately equal numbers of successful and unsuccessful quaternion matches, primarily due to the presence of the Earth or sun in the field of view of one of the sensors. Performance characteristics of the star camera are given in Table 4. The weight savings of this star tracker can be as much as 95% with respect to existing space qualified sensors, and as much as 80% with respect to lightweight versions that still have yet to be flown in space. Clementine used two star cameras to meet reliability and performance requirements, but with the configuration of separate imaging and processing hardware, additional star cameras could have been used, with limited effect on the overall vehicle weight, to improve reliability.

Two small lightweight inertial measurement units (IMUs) were selected for vehicle rate and acceleration measurements. Frequent use of the three-axis star camera allowed the performance requirements for the Clementine gyroscopes to be in the 1 deg/h drift class. This was a significant change from the typical 0.01 deg/h (or better) drift class normally used in precision pointing systems. The addition of a Kalman filter to estimate drift further relaxed the drift specification; this however did not change the selection of the gyroscope package, because the dominant error became gyroscope noise.

In selecting our IMU, we chose two technologies that had not previously experienced the space environment. One unit used interferometric fiber-optic gyroscopes, and the other unit used ring-laser gyroscopes. The first unit was developed for nonspace applications, and the second unit was developed for use in a suborbital flight, making both units far from ideal for a typical space application. To reduce risk, a review of all parts in both units was performed to identify parts that could not survive the expected space environment. No thermal issues were uncovered, and only minor discrepancies in vibration levels; however, there was significant concern in the area of radiation survivability. An extensive search for radiation data for all parts, including some radiation testing, uncovered the need to change several parts. Parts were changed if no radiation data existed, the total dose was extremely low, or there was a possibility of a destructive single-event latchup. With the changes, the units were evaluated to be in the 3–10 krad total-dose range, with the possibility of a nondestructive single event upset or latchup at some point during the mission. The risk associated with a nondestructive upset or latchup was reduced by using both units and having data checking on the output prior to its being used in the ADCS. Specification requirements for the Clementine inertial measurement units are shown in Table 5. The weight savings of these IMUs can be as much as 80% with respect to the smallest existing space-qualified IMUs that are normally used for performance similar to that of Clementine. In terms of cost and schedule, this class of unit could be produced in large numbers with significant reductions in cost and delivery times, compared with existing space-qualified units.

The attitude control system requirements and constraints led to the need for small lightweight reaction wheels for the three-axis precision pointing control system. The reaction wheels selected had no space-flight experience. Reaction-wheel characteristics are provided in Table 6. An earlier version of this wheel used external drive electronics and had half the momentum storage capability. For this mission a weight saving of 15% and a doubling of the momentum storage were realized by switching to internal drive electronics and expanding the reaction-wheel housing. These wheels weigh less than all other space-qualified reaction wheels with the same or even less momentum storage capability. The wheels were mounted so that three were orthogonal and the fourth was a skewed backup. The delivery schedule and cost associated with these wheels was consistent with the smaller, cheaper spacecraft market.

Table 5 IMU specification

Characteristic	Value
Mass	<1 kg
Volume	<50 in.^{3}
Power	<10 W
Gyro max rate	±600 deg/s
Gyro bias accuracy	1 deg/h
Gyro scale-factor accuracy	100 ppm
Gyro random walk	0.25 deg/h$^{1/2}$
Gyro noise	1.5″
Gyro least significant bit	5″
Accel. max acceleration	±30g
Accel. bias accuracy	$10^{-2}g$
Accel. scale-factor accuracy	100 ppm
Accel. noise	1 mm/s
Accel. least significant bit	0.003 ft/s

Table 6 Reaction-wheel performance

Characteristic	Value
Total mass (4 wheels)	11.2 kg
Volume per wheel	150 in.^{3}
Steady-state power (3 active)	28 W
Peak power (3 active)	64 W
Momentum storage	2 N · m · s
Reaction torque	6 oz · in.
Speed range	±2500 rpm

Table 7 ADCS masses

Component	Mass, kg
2 star-tracker cameras	0.6
2 inertial measurement units	1.2
4 reaction wheels	11.1
Total	12.9

The two star cameras, two IMUs, and four reaction wheels provided all the attitude determination and control required to perform the functions of the three-axis precision pointing control system. To meet the attitude determination requirements of spin stabilization, a coarse sun sensor, used primarily by the solar-array drive autotrack system, was used for roll attitude determination at high spin rates. Thrusters were used to provide control torque during both spin stabilization and orbital maneuvers. No other coarse attitude determination sensors were required. As depicted in Table 7, the total system mass of the three-axis precision pointing ADCS hardware is under 13 kg.

IV. Attitude Determination and Control Subsystem

To meet the mission objectives, the Clementine attitude determination and control system had to be capable of performing fine three-axis attitude determination within 0.03 deg and control to within 0.05 deg. This was required for inertial pointing of the payload or high-gain antenna, lunar mapping with the payload, and closed-loop tracking of a star, Earth limb, moon limb, or asteroid. The spacecraft control system also had to be capable of controlling attitude to within 0.5 deg during both short- and long-duration ΔV maneuvers. Finally, the spacecraft had to be capable of performing a

very large solid-rocket-motor burn, which required the addition of control modes associated with stabilization of an unstable spinning body, with spin axis pointing control to within 5 deg and knowledge to within 3 deg.

Attitude Determination

Clementine's two IMUs provided redundant three-axis vehicle inertial rotation information in the form of incremental angles used in a standard quaternion propagation algorithm. The star camera compensated for rate biases along each IMU axis by updating the quaternion estimate every 10 s (nominally). This was accomplished by combining the IMU-based quaternions and the star-camera quaternions in a Kalman filter. On assuming small vehicle rates and error quaternions, the resulting filter algorithm consisted of three two-state, uncoupled Kalman filters with error quaternions and rate biases acting as states. The Kalman filters were amenable to a steady-state solution, and therefore, the gains were chosen as the steady-state values of the time-varying filter analysis. The two filter gains (about each axis) were functions of hardware-based IMU and star-camera noise levels, and designer-based bias process noise levels chosen to obtain desirable bias estimate time histories.

The applicability of the uncoupled fixed-gain Kalman filter lies in the assumption that the vehicle body rates will be low. This assumption was certainly valid in an inertial pointing mode or a lunar mapping mode (in which the body rates were of the order of orbit rate). However, during a relatively fast slew maneuver the body rates would typically invalidate this assumption. During these maneuvers the filter could either be placed in an inactive state (by appropriate settings on the gains) or simply operate in an invalid mode for the duration of the slew, resulting in a transient period upon completion of the slew for the filter to reconverge. For additional detail on the attitude determination system see Ref. 4.

Precision Pointing Control

Clementine used one of six guidance modes and one of two control modes when in three-axis attitude control. The six guidance modes consisted of Earth pointing, lunar mapping, star pointing, inertial pointing, star tracking, and terminal guidance. One control mode used reaction wheels for precision pointing, and the other used thrusters. The thruster control mode was used for all ΔVs and was to be used for precision pointing during the asteroid fly-by. The reaction wheel control mode was used for all other operations. The system-level block diagram is shown in Fig. 4. The solid lines represent measurable or calculated signals, and the broken lines represent unknown signals.

In Earth pointing mode, the spacecraft used the onboard ephemeris to compute the proper attitude quaternion for pointing the spacecraft's high-gain antenna to the center of the Earth or to a specific ground station. This mode was used to transmit the images collected during lunar mapping. When commanded to enter lunar mapping mode, the spacecraft used the onboard ephemeris to compute the command quaternion and body rates for tracking lunar nadir with the payload boresight. An option was available to add a small cross-track offset. Star pointing mode was used to slew and point the payload boresight at a particular star for imaging. The inertial pointing mode allowed a single quaternion with zero body rates, or a table of quaternions and body rates, to be sent up to the control system. It was with this mode that certain targets, such as the Apollo landing sites, were tracked, or special scan profiles performed. The two remaining modes, star tracking and terminal guidance, both used feedback from the payload sensors to adjust the command attitude to maintain track on a star, an Earth limb, a moon limb, or the asteroid.

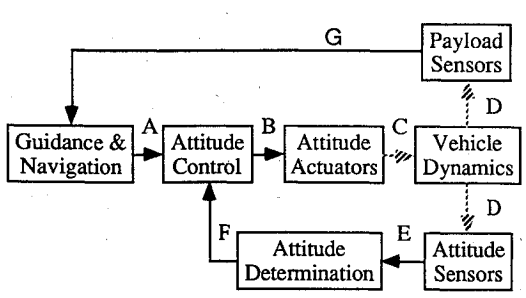

Fig. 4 Block diagram of attitude determination and control system: A—q_c, ω_c; B—u, RW ID, thruster ID; C—torque on vehicle; D—body motion, stars, sun; E—ω, q, a, tref1, tref2; F—q_{IMU}, q_{STC}; and G—image centroid.

The precision pointing control mode used a proportional-integral-derivative control law, with reaction wheels as the primary vehicle actuator. This control mode was used for all guidance modes except when performing the final approach and fly-by of the asteroid and during ΔV maneuvers, situations for which the reaction-wheel torque capability was insufficient. Each axis was treated as independent, with any cross-axis coupling treated as a disturbance source. Any constant (or nearly constant) disturbances such as reaction-wheel friction were handled with the small integral feedback term. For additional detail on the precision pointing control system see Ref. 4.

Large-angle slew logic was used to smooth transitions between modes. This logic was always active, and any required slews were performed autonomously. Whenever a guidance-mode transition command was received, the new commanded attitude quaternion was compared with the current estimated attitude to determine if the change was greater than a preselected limit. If so, then a large-angle rest-to-rest slew maneuver was performed. The large-angle slew algorithms computed the angle of rotation of the vehicle about an Euler axis that would take the vehicle from its current quaternion to the desired quaternion. When using the reaction-wheel control system, a commanded bang-off-bang time history of the slew was then determined such that the wheel speeds and the applied torques stayed within prescribed bounds. When using the thruster control system, slews were performed using simultaneous slew-rate commands about the three body axes to generate a slew rate about the Euler axis. The slew rate was kept low to minimize the fuel consumed executing the maneuver.

The asteroid fly-by phase of the Clementine mission was designed so that the vehicle would have tracked the near-Earth asteroid Geographos with a closest approach distance of 100 km. The terminal guidance mode used for this phase consisted of two feedback loops depicted in Fig. 4. The outer guidance loop provided command signals to the vehicle attitude control system, and the inner control loop provided vehicle torques to follow the commands.

The asteroid flyby guidance loop was designed to generate tracking signals for the vehicle to follow. This loop incorporated a six-state Kalman filter using measurement information from the UV/VIS camera and the LIDAR camera to estimate relative position and velocity between spacecraft and asteroid in inertial space. The camera-based measurements would have occurred at 2.5-s intervals, with a constant-velocity model assumed between measurements. The six states were then converted to the body frame, using the estimated attitude, followed by generation of commanded quaternions and body rates. The inner attitude control loop was designed to follow the quaternion and body-rate commands from the guidance loop. The reaction wheels were used during most of the flyby phase, with thrusters being engaged during the critical 5-min period of closest approach. The thruster logic consisted of simple on–off control with a deadband of 0.03 deg.

Momentum management software was active at all times during operation of the reaction wheels to prevent overspeeding of the wheels. The momentum management system was designed to autonomously monitor reaction-wheel speeds, to determine if a momentum dump was required, and to set up and execute the momentum-dumping thruster pulses. An option was available to command a momentum dump if desired. When a momentum dump was triggered, the system momentum was computed and thruster pulses were fired to reduce the entire system momentum, not just that of a single wheel. With the mission orbits as selected, momentum dumping was expected to occur infrequently during lunar mapping. This was confirmed with on-orbit data: momentum-dumping events occurred once every couple of weeks. Orbit adjustments were performed often enough to effectively dump reaction-wheel momentum when control was switched to thrusters and the wheels were allowed to despin through friction.

Pointing control during ΔVs was performed using the inertial pointing guidance mode and the thruster control mode. The thruster control mode used a bang–bang control system with a pointing-error deadband set at 0.25 deg. Thruster sizing was based on end-of-life thrust levels from the attitude control thrusters and estimated pointing errors of less than 0.1 deg for angular misalignment and 0.12 in. for offset of the 110-lbf thruster. On-orbit data showed that the total effective angular misalignment was between 0.09 and 0.13 deg.

Spin Stabilization

The solid-rocket-motor burn to leave LEO was performed with the spacecraft as a prolate spinner with a spin rate just under 60 rpm. The control requirement for spin-axis pointing was 5 deg with a knowledge requirement of 3 deg. Clementine used the inertial pointing guidance mode to slew the vehicle into position and then used three of four available spin stabilization modes to spin the vehicle up and maintain control and pointing prior to the burn. An open-loop spin-rate change mode was used for spinup to 25 and 50 rpm. The active nutation control mode was used to control nutation-angle growth for approximately 2.5 h at 25 rpm and for approximately 1 h at 50 rpm. The closed-loop spin-rate control mode was used to raise the spin rate up to just under 60 rpm. This spin rate was the maximum for which the solid rocket motor had been qualified, and it provided sufficient gyroscopic stiffness to limit the spin-axis precession during the burn to under 3 deg. A spin-axis precession mode was available to slew the momentum vector after spinup, but was not needed. The solid-rocket-motor burn lasted 63 s, during which time there was no active control of either nutation angle or precession angle. During the burn, the nutation angle increased by 1.6 deg, the precession angle changed by 0.3 deg, and the spin rate increased by only 1.2 rpm. These small changes were consistent with results from spinning-body simulations that included expected solid-rocket misalignments and jet damping terms. Because of the nature of the solid-rocket burn profile (which was approximated as a cylinder burning radially outward), the jet damping terms effectively canceled out the inertia rate-of-change terms, resulting in the minimal spin-rate increase.

Spin attitude determination involved the propagation of the final star-tracker attitude update prior to the spinup, using the IMUs. Knowledge of the spin-axis pointing error was limited by gyroscope errors, the primary contributors being angular random walk for rotations about the transverse axes, and scale factor for the rotation about the spin axis. Knowledge of the spin-axis pointing error was expected to be within 0.25 deg at the end of the first spinup and within 1 deg by the end of the spin period. The computation of the roll orientation was only valid to within 10 deg after spinup to 25 rpm and continued to degrade being based on IMU data only. To maintain knowledge of the roll orientation, the voltage output from the solar array autotrack sun sensors was used as a sun crossing reference. A peak detection algorithm was used to identify the time when the vector to the sun was in a particular plane of the vehicle. With this information, roll orientation accuracy of 10 deg could be maintained, which was sufficient for precession control to an accuracy of 2 deg.

Active nutation control was designed to use spacecraft inertia estimates and IMU outputs to compute and monitor the transverse rates and nutation angle and to operate autonomously. When the nutation angle exceeded a limit of 0.5 deg and the transverse rate exceeded a deadband of 0.01 rad/s, one of two 5-lbf thrusters was fired to drive the transverse rates, and as a result the nutation angle, down to a lower limit of 0.25 deg. The nutation-angle limits, the transverse-rate deadband, and the thruster size were selected to maintain control over a vehicle with a conservative energy dissipation time constant of 25 s at 60 rpm and to minimize momentum-vector walking. From on-orbit data, the energy dissipation time constant was estimated to be 40 s at 57.5 rpm. Momentum-vector walking was less than 1 deg over the 3 h of spin stabilization.

V. On-Orbit Performance

The fine pointing requirements for Clementine included knowledge to within 0.03 deg and control to within 0.05 deg. Figures 5 and 6 show typical combined three-axis pointing errors as a function of time for an Earth-pointing data transmission sequence and a lunar mapping sequence, respectively. Figure 5 shows the attitude determination and control-system fine pointing performance during a period of time in which the following events occurred: a dropout of star-camera updates for 17 min, a Kalman-filter gain change, and a pair of large-angle slews. Prior to the two large-angle slews starting around 110 min, the vehicle was inertially fixed and pointing the high-gain antenna at the Earth for transmission of stored mapping images. Star-camera updates were nominally taken every 10 s. The 17-min period without star updates early in the sequence was a result of the moon obstructing the field of view of the only active star camera. The drift in the attitude during this period is evident upon the return of star-camera updates, at 37 min, with a three-axis pointing-error spike of 0.4 deg. The time (3 min) required to return to normal operation after the spike depends on the Kalman filter rather than the control system. The Kalman-filter gains were fine-tuned at 60 min to improve the three-axis performance, the result being an improvement from 0.075 deg (3σ) to 0.05 deg (3σ) of estimated pointing error. At 110 min, the first large-angle slew oriented the vehicle so that the payload sensors could obtain a series of calibration images. The second slew, at 119 min, oriented the vehicle so that the payload sensors were in position for the next lunar mapping sequence. When comparing performance with and without the star-camera updates, it can be seen that the noise in the system during nominal operation was primarily a result of the star-camera noise rather than the IMU noise. Figure 6 shows the combined three-axis pointing error as a function of time for a lunar mapping sequence. The plot starts and ends with a pair of large-angle slews for sensor calibration imaging and for orientation to lunar mapping or to Earth pointing for data transmission. Between these slews, the performance was better than 0.05 deg (3σ).

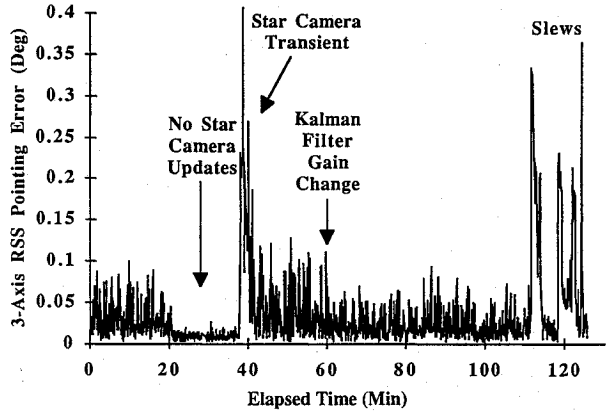

Fig. 5 Pointing performance during inertial pointing.

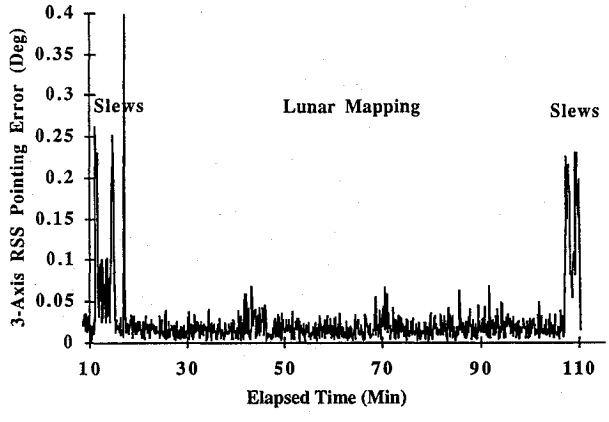

Fig. 6 Pointing performance during lunar mapping.

There were only two hardware anomalies experienced during the mission. The first anomaly was observed through monitoring the bias estimation output of the Kalman filter. From launch through the end of the mission the bias for one of the fiber-optic gyroscopes increased from 3 to 11 deg/h. This change was, on the average, linear

throughout the mission. A reason for this large drift has not been determined. The day-to-day fluctuations in drift were functions of the unit temperature. The slow change in the bias due to temperature fluctuations or the long-term drift of the bias was easily tracked by the Kalman filter and as a result did not affect the fine pointing performance. The second anomaly, a single-event latchup in the ring-laser-gyroscope IMU, was observed when the onboard IMU data-checking logic identified erroneous gyroscope outputs. The latchup increased the noise level on each gyroscope channel in that unit by a factor of 10. After observing the performance for a period of time, power was cycled on the IMU, and the performance returned to normal. The single-event latchup had no effect on the performance of the spacecraft, because the other IMU was active and operating normally.

VI. Conclusions

In this paper we have described how the Clementine spacecraft successfully accomplished a precision pointing mission with control and knowledge requirements of 0.05 and 0.03 deg, respectively, within the severe weight and schedule limitations associated with a mission to the moon and a near-Earth asteroid. In doing so, Clementine provided the first space flight for a new class of small lightweight attitude determination and control hardware, including a new lightweight star camera, new inertial measurement unit technology in small lightweight configurations, and a new small lightweight reaction wheel, all at a fraction of the cost, weight, and schedule of the typical precision pointing control systems for this class of mission. For these components only two anomalies were experienced: a large drift in bias on one of the fiber-optic gyroscopes, and one nondestructive single-event latchup in the ring-laser gyroscope IMU. Neither of these anomalies was catastrophic or detrimental to the mission. The smaller, cheaper, faster concept was demonstrated in that the design, hardware procurement, test, and integration were all performed within two years, of program start and at a fraction of the cost of similar missions.

Acknowledgments

The authors wish to thank Robert Stapleford of Space Applications Corporation in El Segundo, CA, and his staff for their support of the ADCS design, and Samuel Hollander of the Naval Research Laboratory for his review of the manuscript.

References

[1]Rustan, P. L., "Clementine: Mining New Uses for SDI Technology," *Aerospace America*, Jan. 1994, pp. 38–41.

[2]Regeon, P. A., Chapman, R. J., and Baugh, R., "Clementine—the Deep Space Program Science Experiment (DSPSE)," IAA International Conf. on Low-Cost Planetary Missions, Johns Hopkins Univ. Applied Physics Lab., Laurel, MD, April 1994.

[3]Kaufman, B., Middour, J., Dasenbrock, R., and Campion, R., "The Deep Space Program Science Experiment Mission: Astrodynamics Mission Planning," 44th Congress of the International Astronautical Federation, Graz, Austria, Oct. 1993.

[4]Creamer, G., DeLaHunt, P., Gates, S., and Levenson, M., "Attitude Determination and Control of Clementine During Lunar Mapping: Description and On-Orbit Performance," AIAA Guidance, Navigation, and Control Conf., Baltimore, MD, Aug. 1995.

A. L. Vampola
Associate Editor